J Mater Sci: Mater Med (2009) 20:1955–1962
DOI 10.1007/s10856-009-3745-x

Robotic dispensing of composite scaffolds and in vitro responses of bone marrow stromal cells

Seok-Jung Hong · Ishik Jeong · Kyung-Tae Noh · Hye-Sun Yu · Gil-Su Lee · Hae-Won Kim

Received: 23 November 2008 / Accepted: 24 March 2009 / Published online: 14 April 2009

Abstract The development of bioactive scaffolds with a designed pore configuration is of particular importance in bone tissue engineering. In this study, bone scaffolds with a controlled pore structure and a bioactive composition were produced using a robotic dispensing technique. A poly(ε-caprolactone) (PCL) and hydroxyapatite (HA) composite solution (PCL/HA = 1) was constructed into a 3-dimensional (3D) porous scaffold by fiber deposition and layer-by-layer assembly using a computer-aided robocasting machine. The in vitro tissue cell compatibility was examined using rat bone marrow stromal cells (rBMSCs). The adhesion and growth of cells onto the robotic dispensed scaffolds were observed to be limited by applying the conventional cell seeding technique. However, the initially adhered cells were viable on the scaffold surface. The alkaline phosphatase activity of the cells was significantly higher on the HA–PCL than on the PCL and control culture dish, suggesting that the robotic dispensed HA–PCL scaffold should stimulate the osteogenic differentiation of rBMSCs. Moreover, the expression of a series of bone-associated genes, including alkaline phosphatase and collagen type I, was highly up-regulated on the HA–PCL scaffold as compared to that on the pure PCL scaffold. Overall, the robotic dispensed HA–PCL is considered to find potential use as a bioactive 3D scaffold for bone tissue engineering.

Seok-Jung Hong and Ishik Jeong contributed equally.

S.-J. Hong · K.-T. Noh · H.-S. Yu · G.-S. Lee · H.-W. Kim
Biomaterials and Tissue Engineering Lab, Department of Nanobiomedical Science & WCU Research Center, Dankook University, Cheonan, South Korea

I. Jeong · H.-W. Kim (✉)
Department of Biomaterials Science, School of Dentistry & Institute of Tissue Regeneration Engineering (ITREN), Dankook University, Cheonan, South Korea
e-mail: kimhw@dku.edu

1 Introduction

Over the last decade, there has been considerable progress in the development of 3-dimensional (3D) scaffolds for the applications in tissue engineering. Scaffolds should be nontoxic to tissue cells, and provide open-spaced channels for the blood circulation and nutrients supply which is prerequisite for the cell population and further differentiation into specific cell/tissue type [1]. Moreover, appropriate degradability is required to meet the rate of de novo tissue formation. A range of biomedical-grade materials have been developed into tissue engineering scaffolds, which include degradable polymers, bioactive ceramics and their composites [2–8].

Among the methodologies to develop porous scaffolds, recent approaches, including solid freeform fabrication, fused deposition, selective laser sintering, inkjet printing, and robotic dispending, etc., have shown great promise to control the 3D pore configuration [9–17]. The robotic dispensing (RD) method, which is also known as 3D plotting, is a rapid prototyping (RP) technique that utilizes a solution-based material to dispense/inject through a nozzle to draw/construct a 3D scaffold structure using the computer program [18]. The method is potent to construct scaffolds with defined architecture, which affects the initial cell adhesion and migration and the blood and nutrient supply, consequently determining neo-tissue formation [16, 17]. Using the RD technique, a range of compositions, such as degradable polymers (polylactic acid, polyglycolic acid and polycaprolactone) and bioactive ceramics (hydroxyapatite,

tricalcium phosphate and bioglasses) have been fabricated into scaffolds, which retain interconnected pores and a tailored 3D structure [9–15].

Above all, the composites of degradable polymers with bioactive ceramics have gained considerable attention for the applications in bone tissue engineering [7, 19–23]. Recent studies on the composite scaffolds have shown beneficial effects of the bioactive inorganics within the polymer matrices on the bone cell functions, such as enhanced cell adhesion, proliferation and matrix synthesis, as well as on the degradation issue associated with the absorbable polymer component [19–23].

In this study, a degradable and bioactive 3D bone scaffold of polycaprolactone (PCL)/hydroxyapatite (HA) was produced using the RD technique. The processing tools to generate the robotic-dispensed bioactive scaffold are described and the in vitro tissue cell responses to the scaffold are investigated using bone marrow derived stromal cells (BMSCs), as a first criterion to confirm the usefulness of the scaffold in the bone tissue engineering area.

2 Materials and methods

2.1 Robotic dispensing

Commercially available hydroxyapatite (HA, Alfa Aesar) powder was pre-calcined at 900°C for 1 h, milled and sieved down to 45 μm. The HA powders were dispersed in acetone at 50°C by ball-milling for 24 h. Poly(ε-caprolactone) (MW = 80,000, Sigma-Aldrich) was dissolved in HA-acetone solution by vigorous mixing using a ball miller at 50°C. Based on a pilot study, the HA/acetone ratio was determined to be 0.25 by weight, and the PCL/HA ratio was set to 1.

Robotic dispensing into a 3D porous scaffold was performed using robocasting equipment (Ez-ROBO3, Iwashita). The HA–PCL mixture solution was contained in a syringe, which was held by a thermostatically controlled heating jacket set at 50°C. The solution was then injected through a 520 μm diameter needle using a force-controlled plunger to regulate the mass flow rate. A positional control unit linked to a personal computer was operated to direct the fiber dispensing path. As a pilot study, the movement speed of the dispensing fiber was varied (2–13 mm/s) to obtain uniform fiber deposits and well-developed pore structure. By controlling the dispensing program, porous scaffolds could be produced with different pore configurations, such as pore size and porosity. Herein, the intended pore sizes were set to 500 μm × 500 μm on the *xy*-plane by adjusting the interspacing of the injected fibers. The pore dimension along the *z*-axis could be determined by the diameter of the fibers. In particular, deposition was performed onto a cooled ethanol bath to rapidly solidify the HA–PCL composition. After drying, the sample was preheated to 50°C to aid contact fusion of the deposited fibers. Figure 1a shows a schematic diagram of the robotic dispensing set-up used in this study.

The prepared scaffolds were coated with Pt to observe the morphology by scanning electron microscopy (SEM; Hitachi 3000, Japan) under operation conditions of an accelerating voltage 15 kV and magnifications ~20–1000×. The pore configuration was assessed from the SEM-obtained images.

2.2 Cell isolation and culturing

BMSCs were harvested from adult rats (180–200 g, Korea), according to code of practice for the care and use of animals for scientific purposes approved by Animal Ethics Committee, Dankook University School of Medicine. The proximal and distal epiphyses of the femora and tibiae of the rats ($n = 2$) were excised, and the bone marrow was gathered by flushing with a syringe onto a culture flask. The harvested product was centrifuged, and the supernatant was collected and suspended within a culture flask containing α-MEM supplemented with 10% fetal bovine serum and antibiotics (100 U/ml penicillin and 100 mg/ml streptomycin) in a humidified atmosphere containing 5% CO_2 at 37°C. After incubation for 1 day, the medium was refreshed and cultured for up to 7–10 days until the cells reached near confluence.

2.3 Cell viability and growth morphology

For the cell tests, the scaffold prepared with a dispensing speed of 6 mm/s was chosen for its well-developed 3D pore configuration and appropriate pore dimension which supports future tissue engineering application (as deduced from Fig. 1 image and Table 1). The samples prepared with dimensions of ~5 mm × 5 mm × 2 mm were sterilized with 70% ethanol and dried overnight. The cells were seeded on each scaffold (PCL and HA–PCL) and culture dish at a density of 5×10^4 cells/sample, and cultured in an osteogenic medium (the culturing medium described above plus 10 mM β-glycerol phosphate and 50 μg/ml L-ascorbic acid). After culturing the cells for 7 days, the scaffolds were transferred to new culture wells. The CellTiter 96 aqueous one solution cell proliferation kit (MTS assay, Promega) was used to determine the cell viability. The culture medium was removed and a diluted MTS solution was added to each sample and allowed to react for 3 h. A 200 μl aliquot of the reaction sample was used for a colorimetric measurement at A490 nm using a UV-spectrophotometer (Libra S22, Biochrom). Three replicate samples were tested.

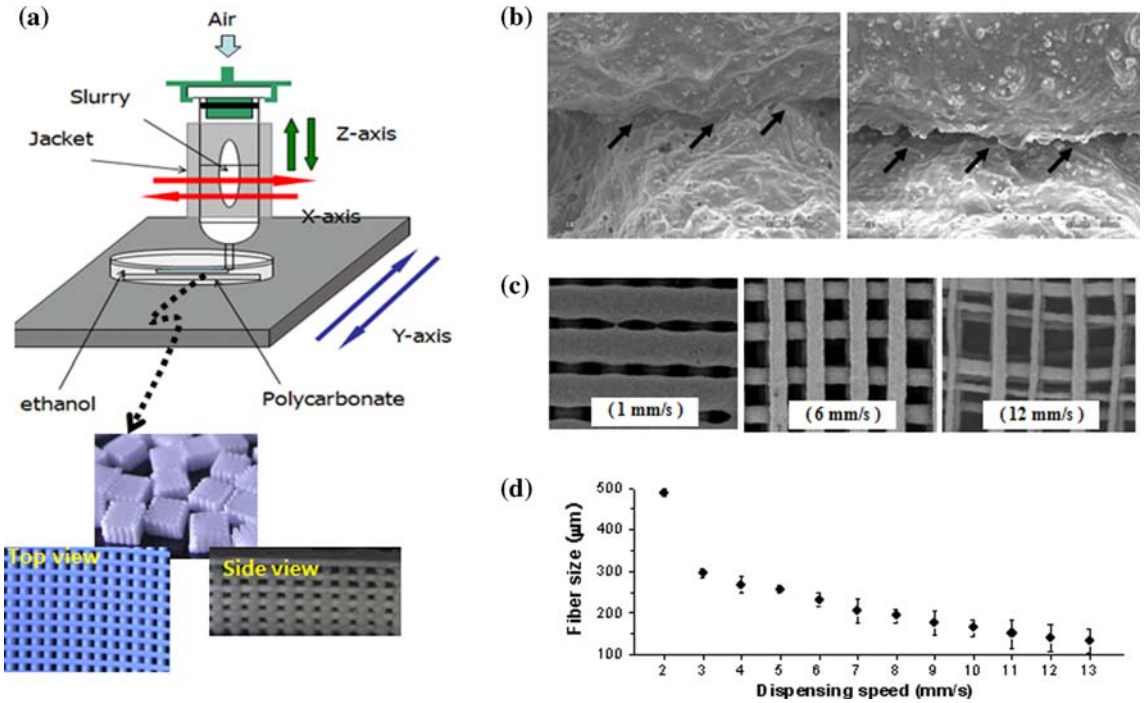

Fig. 1 **a** Schematic diagram of the robotic dispensing system used in this study: HA–PCL slurry contained in a syringe equipped with thermostatic heating jacket was dispensed into a fiber by the air-pressure within the ethanol pool, and the individual fibers were assembled layer-by-layer to a 3D porous scaffold using a computer-aided program. **b** The 3D scaffolds produced were preheated to form fused contacts of individual fibers (*left*), as compared with those not preheated (*right*). **c**, **d** The fiber size was controlled by the *xy*-plane movement speed: the fiber size was decreased with increasing speed

Table 1 Designed and measured configuration of the robotic dispensed PCL and HA–PCL scaffolds

		PCL	PCL–HA
Designed value	*x*-Interval	500	500
	y-Interval	500	500
	z-Interval	200	200
Measured value	*x*-Interval	466 (10)	454 (15)
	y-Interval	451 (8)	446 (17)
	z-Interval	153 (19)	176 (23)
	x-Channel size	260 (9)	222 (29)
	y-Channel size	246 (15)	216 (24)
	z-Channel size	153 (19)	176 (23)
	x-Fiber thickness	206 (12)	232 (16)
	y-Fiber thickness	205 (4)	230 (14)
	z-Fiber thickness	153 (19)	176 (23)

The cell growth morphology was observed by SEM at an accelerating voltage of 15 kV. Cell-scaffold constructs were fixed with glutaraldehyde (2.5%) for 10 min, dehydrated with a graded series of ethanol (75, 90, 95 and 100%) each for 7 min and treated with hexamethyldisilazane for 10 min and sputter-coated with Pt.

Confocal laser scanning microscopy (CLSM; LSM 510, Carl Zeiss) was also used to observe the cells grown on the samples. The cells grown on each sample were fixed with 4% paraformaldehyde, treated with 0.2% Triton X-100, and then blocked with 1% bovine serum albumin (BSA) to prevent nonspecific protein binding. An alexa Fluor 546 phalloidin (invitrogen A22283) solution diluted in PBS was added to each sample to stain F-actin. ProLong® Gold antifade reagent with DAPI (invitrogen P36935) was used to stain the nucleus. A fluorescence image was obtained by CLSM.

2.4 Alkaline phosphatase activity

The alkaline phosphatase (AP) activity was measured to observe the osteogenic differentiation of the BMSCs. The cells were seeded at a density of 5×10^4 cells on each sample (20 mm × 20 mm × 2 mm), and cultured for up to 14 days. The level of AP expression was observed by staining the cell-scaffold constructs using a chemical regent (Takara). After washing with PBS, a fixation solution was added to each sample, which was followed by the addition of the AP reaction substrate. The samples stained in violet were observed by optical microscopy. For the quantification of AP, the cells cultured for 14 days were chosen as a representative example. After culturing, the cell layers were gathered from the scaffolds by disruption with 0.1% Triton X-100 and a further cyclic freezing/

thawing process. The cell lysates were normalized to the total protein content, which was obtained using a DC protein assay kit (BioRad, USA). The AP activity was assessed colorimetrically using a *p*-nitrophenyl phosphate substrate. The enzymatic product *p*-nitrophenol was detected by measuring the optical density (OD) at A410 nm, and the OD value was converted to the AP activity based on a protein standard curve obtained using bovine serum albumin. Three replicate samples were tested.

2.5 Gene expression by real-time PCR

At the culturing period of 10 days, the expression of the bone-associated genes, including collagen type I and alkaline phosphatase, was confirmed by quantitative real-time polymerase chain reaction (PCR). After isolation, RNA was converted to cDNA and amplified. Accumulation of PCR products was monitored and quantified using SYBR GreenER qPCR SuperMix reagents (Invitrogen) and the comparative CT method in which the accumulated PCR products for each of the genes examined is normalized to the housekeeping gene GAPDH. Primer sequences were as follows: ALP forward: 5′- GTCTGGAACCGCACTGA ACT C-3′, reverse: 5′-CCAGCAAGAAGAAGCCTTTG-3′; COL forward: 5′-CTGGCAAGAACGGAGATGAT-3′, reverse: 5′-TTAGGACCAGCAGGACCAGT-3′; GAPDH forward: 5′-AAACCCATCACCATCTTCCA-3′, reverse: 5′-GTGGTTCACACCCATCACAA-3′. Two replicate samples were tested.

2.6 Statistical analysis

The data was represented as the mean ± one standard deviation. Statistical analysis was carried out using one-way ANOVA followed by a Bonferroni correction. The significance level was set to $P < 0.001$.

3 Results and discussion

3.1 Robotic dispensed bioactive scaffolds

As shown in Fig. 1a, the 3D scaffolds with an adjusted pore configuration could be generated by the fiber deposition in the *xy*-plane, and in the *z*-axis with a layer-by-layer assembly process using the robocasting equipment. The slurry properties are of particular importance for the success of the fiber deposition and 3D assembly. Herein, the HA was calcined and milled to a fine powder in order to improve the rheological properties. In practice, the initial HA nanopowders, when not being calcined, could be loaded at limited levels in acetone, which hampered the easy fabrication of the fiber injection. When the powders were calcined and milled to fine powders, the powder characteristics provided the appropriate slurry properties for the HA–PCL mixture and subsequent fiber deposition. The use of a heating jacket set at an elevated temperature (50°C) assisted in dispensing the fibers with a uniform size. The deposition pool where the fiber was ejected should also be carefully set in order to aid fiber formation. Herein, the ethanol used was found to be beneficial in allowing rapid solidification of the HA–PCL mixture slurry and maintaining the fiber morphology. In addition, a preheating treatment at low temperature was required to integrate the individual fibers into a 3D scaffold through a layer-by-layer process.

The SEM image in Fig. 1b showed the effect of the preheating treatment (at 50°C for 10 min) on the contact fusion of the individual fibers, which resulted in a mechanically stable 3D scaffold without disintegration of each layer. The uniformity and size of the fibers were also controlled by the speed of the *xy*-plane movement (shown in Fig. 1c, d). At low speed, the injected fibers were held together with the adjacent fibers, resulting in the disintegration of the fiber morphology (1 mm/s in Fig. 1c). At appropriate speeds, well-developed cylindrical fibers could be generated (6 mm/s in Fig. 1c). However, as the speed increased to 12 mm/s, the fiber thickness was variable depending on the position, resulting in nonuniform fibers. The change in fiber thickness with respect to the speed was presented in Fig. 1d. Data showed a linear decrease in the fiber thickness with increasing the speed. Herein, the speed was determined to 6 mm/s to generate fibers with thicknesses of approximately 200–230 μm. Consequently, control of the slurry characteristics and the fiber formation was prerequisite to constructing 3D scaffold with well-developed pore configuration. The shape and pore configuration were further controlled using a 2D fiber-assembling process and 3D layer-integration step, which were controlled by the computer-aided program.

Table 1 summarizes the designed and measured values of the pore configurations of the robotic dispensed PCL and HA–PCL scaffolds. The intervals of the fiber deposition along the *xy*-plane and the vertical *z*-axis were set to 500 and 200 μm, respectively. However, the measured values were slightly reduced to approximately 450–480 μm and 150–180 μm, respectively. Along the *xy*-plane, the fiber thicknesses of PCL and HA–PCL were measured to be approximately 230 and 210 μm, respectively. Along the *z*-axis, the thicknesses of PCL and HA–PCL were approximately 150 and 180 μm, respectively. The smaller fiber thicknesses along the *z*-axis with respect to those along the *xy*-plane were attributed to vertical suppression by gravity, and the larger fiber thicknesses in the HA–PCL with respect to those in PCL are believed to be due to

differences in the slurry properties or in the solidification rate during deposition. Consequently, the pore channel sizes for PCL along the *xy*-plane and *z*-axis were approximately 250–260 μm and 150 μm, respectively. For HA–PCL the pore channel sizes along *xy*-plane and *z*-axis were approximately 220 and 180 μm, respectively. In the design of the pore channels, it should be noted that the channel size along the *xy*-plane decreases with increasing fiber thickness while the trend is reverse along the *z*-axis. The channel sizes obtained herein were considered to be suitable to aid the vascularization and cell migration, which is at least prerequisite for the 3D scaffold in tissue engineering. In practice, the 3D pore configuration of the scaffold is adjustable by changing the RD processing parameters, which definitely influences the scaffold performance in view of biological and mechanical functions. Therefore, the elucidation of the relationship between pore configuration and scaffold performance is of special importance to gain optimal designing and scaffold fabrication tools to target bone tissue. Regarding this issue, further work is needed using different pore configurations, such as pore size, porosity and pore connectivity.

Figure 2 shows the morphology of the robotic dispensed HA–PCL scaffold. The electron macroscopic views taken along the *xy*-plane (Fig. 2a, c) and *z*-axis (Fig. 2b) showed the formation of fibers and square channels well. An enlarged morphology of the fiber surface (Fig. 2d) showed the presence of HA powders with sizes less than a few micrometers embedded uniformly within the PCL matrix.

3.2 rBMSCs responses

Rat bone marrow derived stromal cells (rBMSCs) were isolated and cultured on the robotic dispensed 3D scaffolds, and the cell growth and osteogenic differentiation behaviors were observed. Figure 3 shows the morphology of the cells grown on the PCL and HA–PCL scaffold for 7 and 14 days of culturing. At day 7, the SEM images showed the presence of cells on both types of scaffolds, which are in intimate contact with the underlying substrates (Fig. 3a, b) for PCL and d, e for HA–PCL). The CLSM images revealed active cytoskeletal extensions of the cells and stained nuclei (Fig. 3c for PCL and f for HA–PCL). At day 14, significant cell growth was observed on both types of scaffolds, where the cells formed a layer covering the scaffold surface (Fig. 3g for PCL and h for HA–PCL). Similar growth morphology was observed for both types of scaffolds.

Cell growth at day 7 was assessed by the MTS cell viability, as shown in Fig. 4. There was no significant difference in cell growth observed between PCL and HA–PCL scaffolds ($P > 0.05$), even though the data showed a slightly higher level in the HA–PCL scaffold. However, the cell viability was significantly lower on the both types of 3D scaffolds with respect to that on the control (culture dish) (Fig. 4a). This was due to the large quantity of seeded cells settling to the bottom of the culture dish bypassing the pore channels of the scaffolds. Many cells that adhered to the bottom of the culture dish and grew

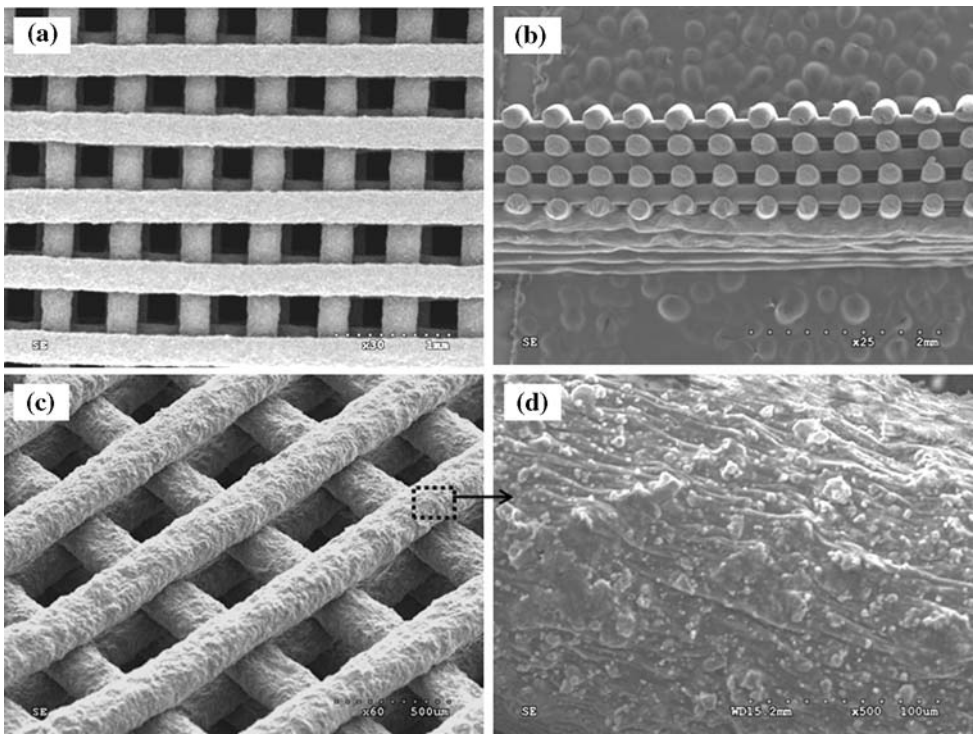

Fig. 2 SEM images of the robotic dispensed HA–PCL bone scaffolds: **a** *xy*-plane horizontal view and **b** *z*-axis vertical view. **c** tilted view of **a**, showing well-developed straight fibers and open-channeled pores. **d** microstructure of the fiber stem in **c**, revealing the hydroxyapatite particles distributed in the PCL matrix

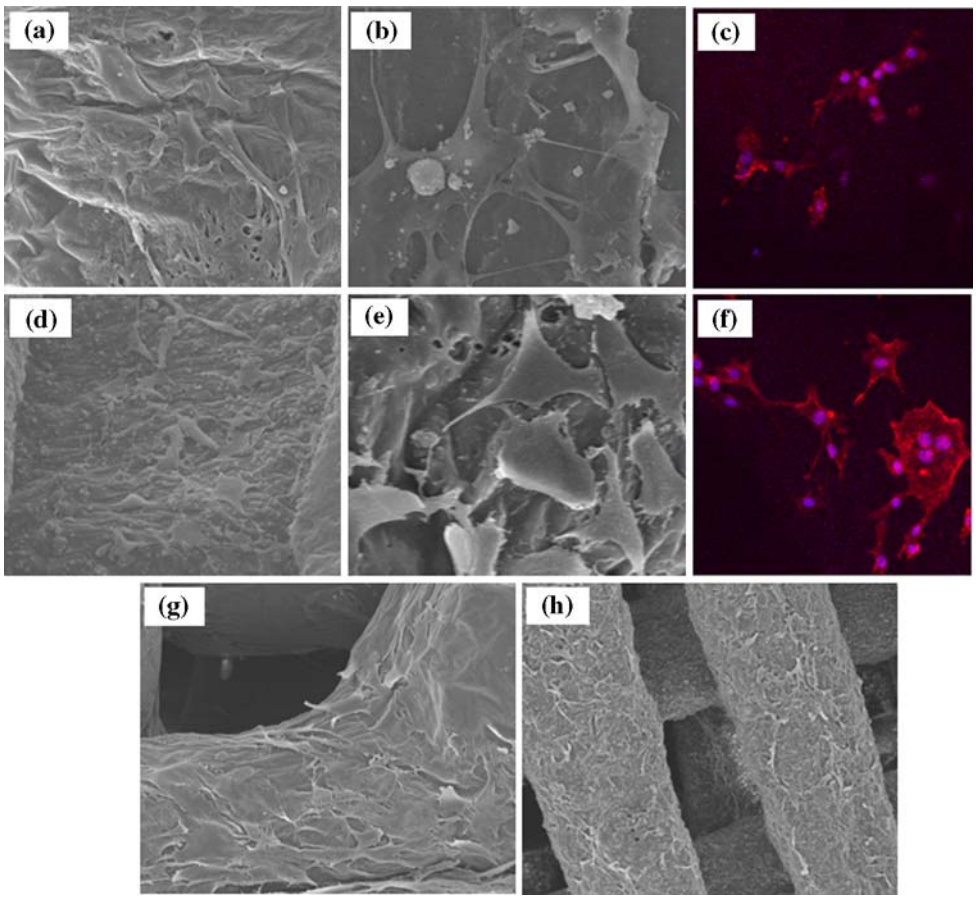

Fig. 3 BMSCs growth morphology upon the 3D scaffolds of PCL (**a**–**c**, **g**) and HA–PCL (**d**–**f**, **h**), as observed by SEM and CLSM: At day 7 (**a**–**f**), the cells were viable in intimate contact with the underlying fiber stems (PCL: **a**, **b** and HA–PCL: **d**, **e**). CLSM revealed the cell nuclei and cytoskeletal process (PCL: **c** and HA–PCL: **f**). At day 14, the cells proliferated actively on both scaffolds, covering most the fiber stems completely (PCL: **g** and HA–PCL: **h**)

during the culturing period were easily observed. Therefore, a fraction of the cells that adhered directly to the surface of the scaffold should contribute to the MTS result because the cell-scaffold construct was transferred to a new culture well for assay. For this reason, another set of the MTS experiments were carried out to include the cells present on the bottom of the culture dish, which showed that the level of cell growth was similar and even slightly higher than that of the culture dish control (Fig. 4b). Therefore, the culturing method used in this study required further development in order to improve the initial cell adherence. A culture system involving the circulation of a cell source for uniform adhesion and further 3D vascularization for an active cell growth is required [24–26], which is currently in progress. These results suggest that the cells initially adhering to the scaffold surface grew actively and were viable to the level of the culture dish, forming a thick cell layer on the scaffolds. This shows that the bioactive scaffolds should retain cellular compatibility providing a favorable substrate condition for the cells to populate on.

Further osteogenic differentiation of the cells was assessed by determining the alkaline phosphatase (AP) activity. The AP enzyme is intimately involved in the relatively early stages of bone cell differentiation and mineralization, and is a useful marker for osteogenic pathway for the osteoprogenitor/stem cells. Figure 5a shows the AP-stained images of the cell-scaffold constructs, after culturing for 7 and 14 days. Clear differences in the violet color stain were observed between the PCL and HA–PCL scaffolds, i.e., much darker violet staining on the HA–PCL scaffold for both periods. The quantitative AP result demonstrated significantly higher AP activity in the rBMSCs on the HA–PCL scaffold than on the PCL scaffold (Fig. 5b). Moreover, the PCL scaffold showed a better AL level than the culture dish. Based on this, the HA–PCL scaffold is believed to offer better substrate conditions for the rBMSCs to be modulated into an osteogenic differentiation. The incorporated HA should play a stimulatory role in the differentiation of rBMSCs by altering the cellular microenvironment, such as increasing the released ionic level and altering the surface properties.

The expression of a series of bone-associated genes, including collagen type I and alkaline phosphatase, was assessed on both types of the robotic dispensed scaffolds by using real-time PCR, as shown in Fig. 6. At the culturing period of 10 days, the rBMSCs showed significantly higher level of gene expressions upon the HA–PCL scaffold than on the PCL scaffold (by a factor of $\sim$10). The result

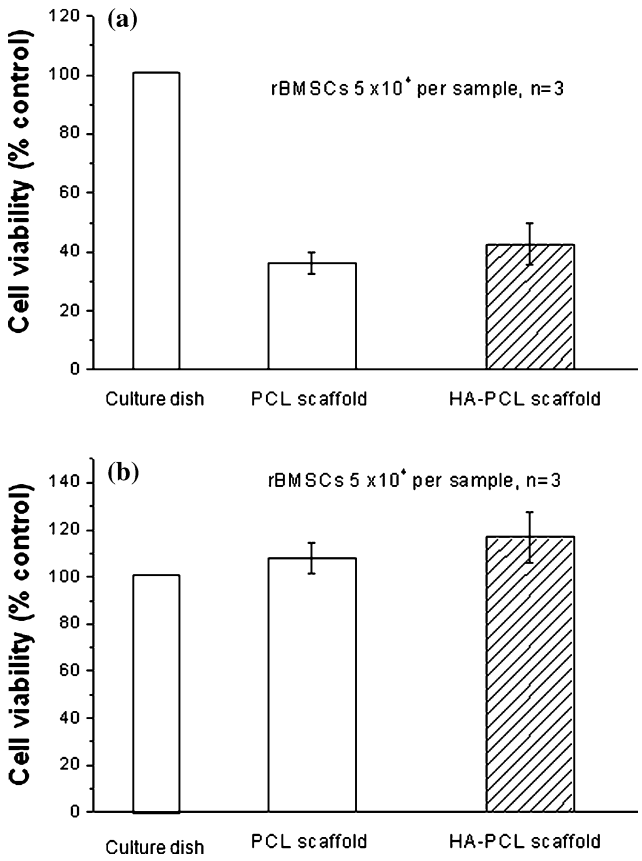

Fig. 4 Cell viability on the 3D bone scaffolds after culturing for 7 days, as assessed by the MTS method: **a** cells only adhered to the scaffolds were assessed by transferring the scaffold samples to a new culture plate, whilst **b** cells grown on the bottom of the culture wells bypassing the pore channels of the scaffolds were also assessed

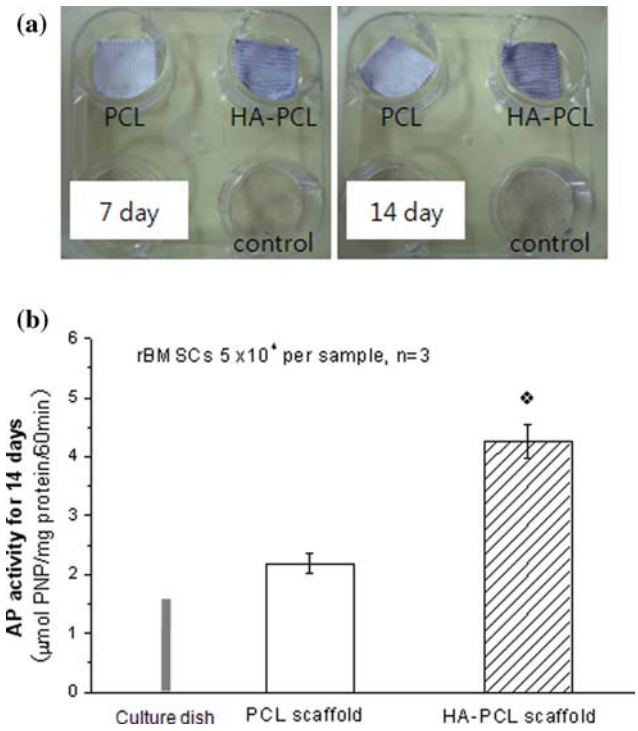

Fig. 5 **a** AP staining image of the cell-scaffold constructs (PCL and HA–PCL) after culturing for 7 and 14 days, showing much darker violet in the cells on the HA–PCL scaffold for both periods. **b** AP activity expressed by the cells was quantified at day 14, as a representative time point. One-way ANOVA followed by Bonferroni correction showed statistical significance at $^{*}P < 0.001$

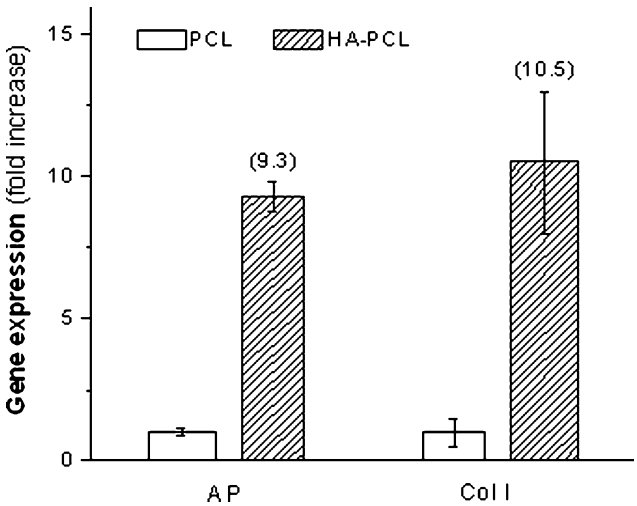

Fig. 6 Real time PCR showing the expression of collagen type I and alkaline phosphatase upon the robotic-dispensed 3D scaffolds of PCL and HA–PCL at the culturing time of 10 days. Significantly higher stimulation of gene expressions was noticed on the HA–PCL than on the PCL

suggested the developed HA–PCL scaffold should better support the bone marrow mesenchymal stem cells to undergo osteogenic pathway, and thus hold greater potential to be used as bone tissue engineering scaffolds.

Based on the results, the robotic dispensed HA–PCL bioactive scaffold is considered to provide cell compatible substrate conditions that can stimulate rBMSCs into osteogenic differentiation, and thus have potential applications as a 3D matrix for bone tissue engineering. Currently, further experiments are underway to determine the optimal culturing conditions for the cell adhesion and population using dynamic perfusion culture system for real tissue engineering applications of the designed scaffolds.

4 Conclusions

Poly(ε-caprolactone) (PCL)–hydroxyapatite (HA) bioactive scaffold with a designed pore structure was produced using a computer-aided robocasting technique. The slurry deposition into individual fibers and the subsequent layer-by-layer integration should be controlled carefully in order to construct a uniform and stable 3D structure. The rat bone

marrow stromal cells (rBMSCs) showed limited adhesion to the 3D scaffolds by the conventional 2D cell culturing method. However, the adhered cells were viable and reached the level of growth observed on the culture dish. In particular, the HA–PCL scaffold was found to stimulate the osteogenic differentiation of rBMSCs according to the measured alkaline phosphatase activity and bone-associated gene expressions. Overall, the robotic dispensed HA–PCL scaffold has potential applications as a bioactive matrix in the bone tissue engineering field.

Acknowledgement The authors thank Prof. Jang JH for his assistance in the gene expression study.

References

1. Hutmacher DW. Scaffold in tissue engineering bone and cartilage. Biomaterials. 2000;21:2529–43. doi:10.1016/S0142-9612(00)00121-6.
2. Lu L, Zhu X, Valenzuela RG, Currier BL, Yaszemski MJ. Biodegradable polymer scaffolds for cartilage tissue engineering. Clin Orthop Relat Res. 2001;391:S251–70. doi:10.1097/00003086-200110001-00024.
3. Kim HW, Shin SY, Kim HE, Lee YM, Chung CP, Lee HH, et al. Bone formation on the apatite-coated zirconia porous scaffolds within a rabbit calvarial defect. J Biomater. 2008;28:485–504.
4. Jones JR, Ehrenfried LM, Hench LL. Optimising bioactive glass scaffolds for bone tissue engineering. Biomatrials. 2006;27:964–73.
5. Kim HW, Lee SY, Bae CJ, Noh YJ, Kim HM, Ko JS, et al. Porous ZrO2 bone scaffold coated with hydroxyapatite with fluorapatite intermediate layer. Biomaterials. 2003;23:3277–84.
6. Rezwan K, Chen QZ, Blaker JJ, Boccaccini AR. Biodegradable and bioactive porous polymer/inorganic composite scaffolds for bone tissue engineering. Biomaterials. 2006;27:3413–31. doi:10.1016/j.biomaterials.2006.01.039.
7. Kim HW, Knowles JC, Kim HE. Hydroxyapatite/poly(ε-caprolactone) composite coatings on hydroxyapatite porous bone scaffold for drug delivery. Biomaterials. 2004;25:1279–87.
8. Stevens MM. Biomaterials for bone tissue engineering. Mater Today. 2008;11:18–25. doi:10.1016/S1369-7021(08)70086-5.
9. Lu L, Mikos A. The importance of new processing techniques in tissue engineering. MRS Bull. 1996;21(11):28–32.
10. Yang S, Leong K, Du Z, Chua C. The design of scaffolds for use in tissue engineering. Rapid prototyping techniques. Tissue Eng. 2002;8:1–11. doi:10.1089/107632702753503009.
11. Hutmacher DW, Schantz T, Zein I, Ng KW, Teoh SH, Tan KC. Mechanical properties and cell cultural response of polycaprolactone scaffolds designed and fabricated via fused deposition modeling. J Biomed Mater Res. 2001;55(2):203–16. doi:10.1002/1097-4636(200105)55:2<203::AID-JBM1007>3.0.CO;2-7.
12. Dellinger JG, Cesarano JIII, Jamison RD. Robotic deposition of model hydroxyapatite scaffolds with multiple architectures and multiscale porosity for bone tissue engineering. J Biomed Mater Res A. 2007;82A:383–94. doi:10.1002/jbm.a.31072.
13. Koh YH, Jun IK, Kim HE. Improved compressive strength of reticulated porous zirconia using carbon coated polymeric sponge as novel template. Mater Lett. 2006;60:2507–10. doi:10.1016/j.matlet.2005.10.103.
14. Miranda P, Saiz E, Gryn K, Tomsia AP. Sintering and robocasting of B-tricalcium phosphate scaffolds for orthopaedic applications. Acta Biomater. 2006;2:457–66. doi:10.1016/j.actbio.2006.02.004.
15. Woodfield TBF, Malda J, de Wijin J, Peters F, Riesle J, van Blitterswijk CA. Design of porous scaffolds for cartilage tissue engineering using a three-dimensional fiber-deposition technique. Biomaterials. 2004;25:4149–61. doi:10.1016/j.biomaterials.2003.10.056.
16. Hollister SJ, Maddox RD, Taboas JM. Optimal design and fabrication of scaffolds to mimic tissue properties and satisfy biological constraints. Biomaterials. 2002;23:4095–103. doi:10.1016/S0142-9612(02)00148-5.
17. Hutmacher DW, Sittinger M, Risbud MV. Scaffold-based tissue engineering: rationale for computer-aided design and solid free-form fabrication systems. Trends Biotechnol. 2004;22:354–62. doi:10.1016/j.tibtech.2004.05.005.
18. Chua CK, Leong KF, Lim CS. Rapid prototyping. 2nd ed. Singapore: World scientific; 2003.
19. Kim HW, Kim HE, Salih V. Stimulation of osteoblast responses to biomimetic nanocomposites of gelatin–hydroxyapatite for tissue engineering scaffolds. Biomaterials. 2005;26:5221–30.
20. Liu L, Xiong Z, Yan Y, Hu Y, Zhang R, Wang S. Porous morphology, porosity, mechanical properties of poly(-hydroxy acid)-tricalcium phosphate composite scaffolds fabricated by low-temperature deposition. J Biomed Mater Res A. 2007;82A:618–29. doi:10.1002/jbm.a.31177.
21. Habraken WJEM, Wolke JGC, Jansen JA. Ceramic composites as matrices and scaffolds for drug delivery in tissue engineering. Adv Drug Deliv Rev. 2007;59:234–48. doi:10.1016/j.addr.2007.03.011.
22. Kim HW, Knowles JC, Kim HE. Effect of biphasic calcium phosphates on drug release and biological and mechanical properties of poly (ε-caprolactone) composite membranes. J Biomed Mater Res A. 2004;70A:467–79.
23. Shor L, Güçeri S, Wen X, Gandhi M, Sun W. Fabrication of three-dimensional polycaprolactone/hydroxyapatite tissue scaffolds and osteoblast-scaffold interactions in vitro. Biomaterials. 2007;28:5291–7. doi:10.1016/j.biomaterials.2007.08.018.
24. Martin I, Wendt D, Heberer M. The role of bioreactors in tissue engineering. Trends Biotechnol. 2004;22(2):80–6. doi:10.1016/j.tibtech.2003.12.001.
25. Pei M, Solchaga LA, Seidel J, Zeng L, Vunjak-Novakovic G, Caplan AI, et al. Bioreactors mediate the effectiveness of tissue engineering scaffolds. FASEB J. 2002;16:1691–4.
26. Solchaga LA, Tognana E, Penick K, Baskaran H, Goldberg VM, Caplan AI, et al. A rapid seeding technique for the assembly of large cell/scaffold composite constructs. Tissue Eng. 2006;12(7):1851–63. doi:10.1089/ten.2006.12.1851.